CLAUS S. JACOBSEN

Infrared Studies on the Electronic Structure of Organic Conductors

ABSTRACT. *It is experimentally shown that a simple Drude analysis of the reflectance edge in organic conductors yields reliable values for electronic transfer integrals. The integrated infrared oscillator strength is found to be smaller than expected from band theory. The reduction is interpreted as being an effect of the short range electron-electron interaction and is used to compare the strength of this interaction among different materials. It is concluded that highly correlated systems may be semiconductors due to electron-phonon driven instabilities, or, if the interstack coupling is sufficient, may remain good metals to low temperatures. The role of the electron-molecular vibration coupling is stressed, both as contributing to instabilities, and as a microscopic probe.*

Physics Laboratory 3, Technical University of Denmark,
DK-2800 Lyngby, Denmark.

Introduction

An ordinary metal, like copper, is characterized by two basic features: (1) A high concentration of valence electrons, which are in principle free to move through the metal, and (2) a strong overlap of the valence electron orbitals (wavefunctions) on neighbour atoms, which effectively makes the electrons delocalize in the metal. The only force capable of inhibiting the free motion of the electrons is the direct Coulomb repulsion between the negatively charged particles. If strong enough, such a repulsion would localize the electrons, one on each atom (Mott, 1949). Although the arguments are quite complicated, it is now well understood, how the electronic system itself almost completely screens out the Coulomb repulsion. The effectiveness of the screening is due to the same two features listed above: A high carrier density and a good neighbour contact. As a consequence ordinary metals have high electrical conductivities (e.g. copper at room temperature with $\sigma = 6\times10^5$ Scm^{-1}).

Furthermore, the conductivity increases when the metal is cooled, since the scattering rate for the electrons decreases as the thermally induced vibrations of the atoms get smaller in amplitude. Some metals

even become superconducting at very low temperatures (a few Kelvin), that is, their electrical resistivity vanishes completely.

Such behaviour is contrasted by semiconductors like silicon, where the charge carriers are thermally excited from a state which is insulating at low temperatures. All electrons take part in the localized crystal binding. Thus typically, the conductivity of semiconductors increases with temperature.

In a recently very active, interdisciplinary field of the materials sciences, chemists and physicists have attempted to mimic metallic, electrical properties in organic compounds. The long term perspective is to make it possible employing the great flexibility of organic chemistry to design, synthesize, and manufacture materials with specific, desirable properties.

Presently, there are two approaches to the synthetic metal problem. A considerable amount of effort goes into attempts of doping to high levels polymeric semiconductors like polyacetylene, $(CH)_x$ (for a review see, for example, Baeriswyl et al. (1982)). Although promising for applications, such materials are not truly metallic, since their carrier concentrations are fairly low.

The other approach has lead to the large class of materials, normally called organic conductors (see, for example, Jerome and Schulz (1982), and references therein). Here the work has been directly aimed at incorporating the two basic features of a metal into crystals of organic molecules. The high concentration of charge carriers is obtained by bringing together at least two species of molecules, one which is willing to accept an extra, unpaired electron (acceptor molecule), and another which readily gives up an electron (donor molecule). Thus in the crystal, charge is transferred from donors to acceptors. The second feature, good contact between neighbour building blocks, i.e. the molecules, is achieved by using near planar, π-bound organic molecules, which tend to form stacks with a fair inside overlap. It follows that the contact between stacks must be rather weak, hence the materials are electrically highly anisotropic. In some contexts, they may even be designated one-dimensional (1D).

Thus to shortly characterize organic conductors, they are synthetic materials, which by elementary solid state physics are expected to be metals in electrical sense. However, they are highly anisotropic, have carrier densities one or two orders of magnitude below those of ordinary metals, and even along the molecular stacks, the neighbour contact is at least ten times weaker than in, for example, copper. The latter features

arise from the use of rather big building blocks, which do not pack as effectively as compact metal atoms.

Therefore, it is not surprising that organic conductors so far have been found to be inferior to the elements with respect to metallic quality. The first organic conductors were in fact semiconducting. These early studies date back to the 1950s and -60s (see Gutmann and Lyons, 1967). In 1973 the first material with genuine metallic properties was synthesized (Ferraris et al., 1973). TTF-TCNQ has a room temperature conductivity of order 600 Scm^{-1}, and a strongly increasing $\sigma(T)$ down to 60K. However, below 60K a metal-insulator transition destroys the conductivity. In the following years many derivatives of TTF-TCNQ were studied, and in 1980 Jerome et al. reported superconductivity in the material $TMTSF_2PF_6$ (below 1K and only under a pressure of ~10 kbar). The present state of art involves several ambient pressure superconductors (working up to 2.5K), as well as materials with a wide range of interesting magnetic and non-magnetic ground states. Many of the metal-insulator and magnetic phase transitions may be related to the low-dimensionality of the materials. Thus while applications are still somewhat in the future, the materials constitute extremely interesting model systems for solid state physics.

It is the aim of the present study to use infrared (IR) spectroscopy in characterizing the basic interactions in organic conductors. We shall discuss how the IR properties give direct information on the intra- as well as interstack contacts, on the interplay between electron-electron and electron-vibration interactions, and to some extent on the detailed nature of the phase transitions occuring in these materials. It is a central result of the study, that the short range electron-electron interaction plays a role far more important than in ordinary metals. It indeed appears that the probability for finding two conduction electrons on the same molecule is quite small in several materials. The electrons then more or less behave as spinless fermions in transport and optical properties.

Although essential for a microscopic understanding of the electronic structure, the electron-electron interaction needs not destroy the metallic state. Even the organic superconductors appear to have a sizeable electron-electron Coulomb interaction, but a large interchain overlap reduces its impact on the physical properties.

Materials and methods

All the materials investigated in this study belong to the group of potential metals, which are characterized by partially filled one-electron bands and no strong static disorder. The constituent organic molecules are shown in Fig. 1, and their systematic names are listed in Table I.

We will deal with two groups of compounds. (1) The doublestack conductors, like TTF-TCNQ, have uniform stacks, and donor as well as acceptor chains have unpaired electrons. The crystal structure is sketched in Fig. 2(a). A key parameter for these materials is the degree of charge transfer, ϱ, equal to the average number of carriers per molecule. ϱ is determined by a complicated energy balance (Torrance, 1979), and is best found indirectly by diffuse X-ray scattering, which detects weak superstructures related to the Fermi wavevector. (2) The singlestack conductors, dealt with here, are complex salts, where the stoichiometry is such that there is one closed shell ion for a pair of organic molecules. The counterion may be organic or inorganic, but ϱ for the conducting

Table I. Organic molecules. D = donor. A = acceptor

Abbr.	Type	Systematic name
TTF	D	$\Delta^{2,2'}$-bi-1,3-dithiolylidene
TMTTF	D	$\Delta^{2,2'}$-bi-4,5-dimethyl-1,3-dithiolylidene
DBTTF	D	$\Delta^{2,2'}$-bibenzo-1,3-dithiolylidene
HMTTF	D	$\Delta^{2,2'}$-bicyclopenteno-1,3-dithiolylidene
TSF	D	$\Delta^{2,2'}$-bi-1,3-diselenolylidene
TMTSF	D	$\Delta^{2,2'}$-bi-4,5-dimethyl-1,3-diselenolylidene
DBTSF	D	$\Delta^{2,2'}$-bibenzo-1,3-diselenolylidene
HMTSF	D	$\Delta^{2,2'}$-bicyclopenteno-1,3-diselenolylidene
BEDT-TTF (ET)	D	$\Delta^{2,2'}$-bi-5,6-dihydro-1,4-dithiino-1,3-dithiolylidene
MEM^+	D[a]	N-ethyl-N-methyl-morpholinium
TCNQ	A	7,7,8,8-tetracyano-p-quinodimethane
DMTCNQ	A	2,5-dimethyl-7,7,8,8-tetracyano-p-quinodimethane
$TCNQC1_2$	A	2,5-dichloro-7,7,8,8-tetracyano-p-quinodimethane
$TCNQF_4$	A	2,3,5,6-tetrafluoro-7,7,8,8-tetracyano-quinodimethane
TNAP	A	11,11,12,12-tetracyanonaphto-2,6-quinodimethane

[a] closed shell ion

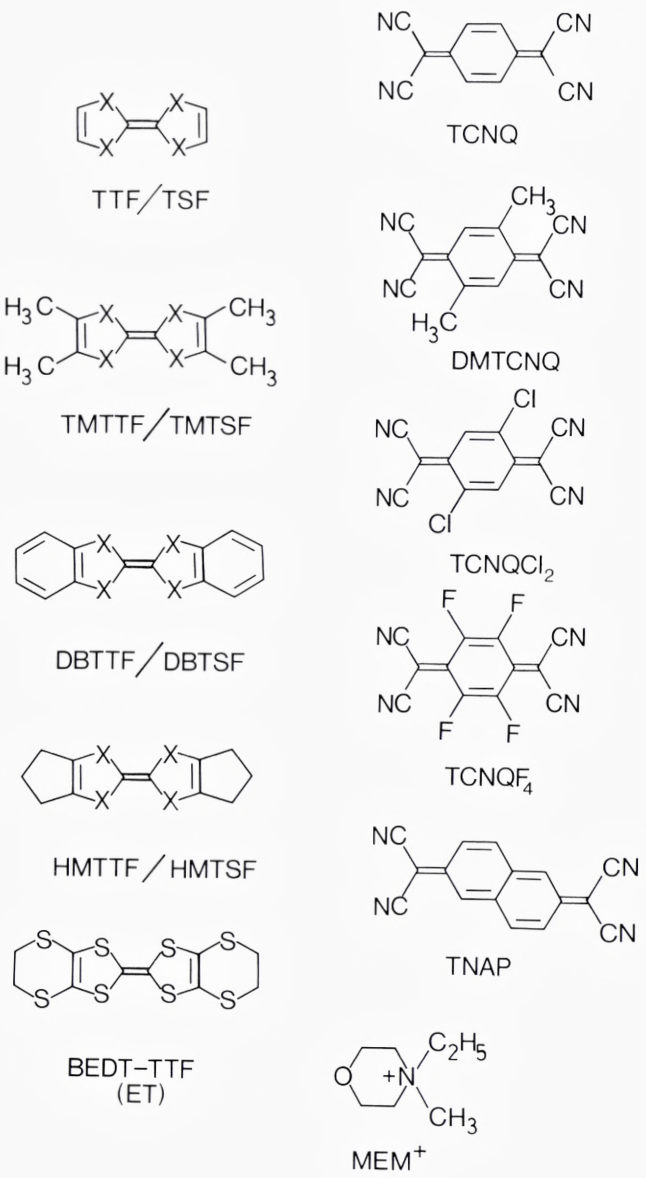

Fig. 1. Donor and acceptor molecules (cfr. Table I).

stack is always 0.5. Due to the stoichiometry alone the stacks show some dimerisation. A typical structure is sketched in Fig. 2(b).

Table II lists the relevant materials with basic physical properties, and gives references to more detailed information.

The organic conductors are usually available as small, 2-4 mm long needles with cross-sectional dimensions of a few tenths of a mm. The

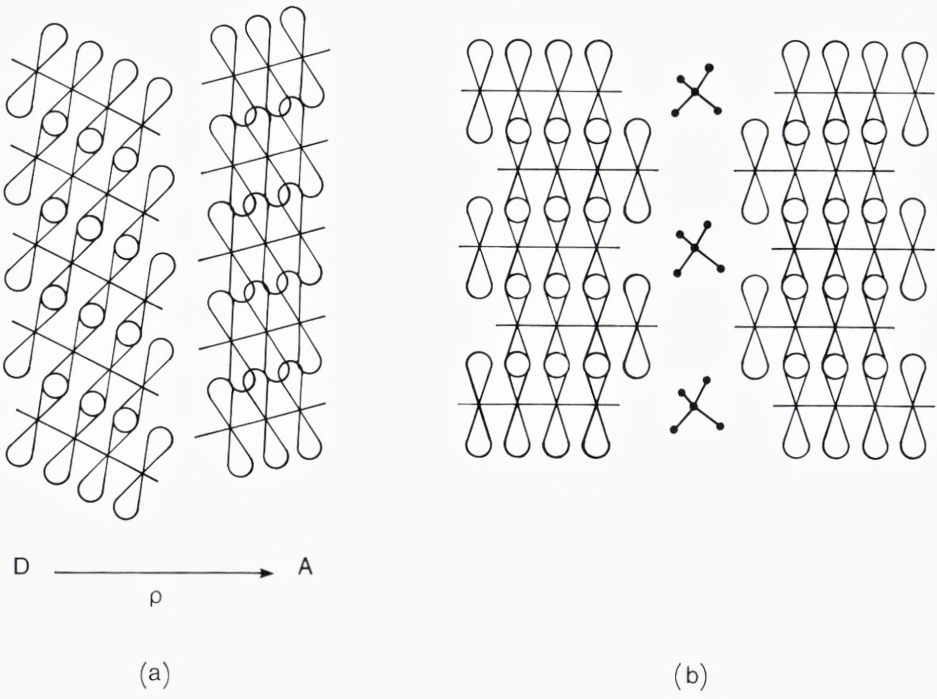

Fig. 2. Schematic crystal structures. (a) Double-stack conductor. ϱ is the degree of charge transfer. (b) Single-stack conductor with inactive counterions.

faces tend to be of high optical quality, and since the crystals are opaque in the entire range, studies of the IR properties are best conducted as specular, polarized, near-normal incidence reflectance measurements. Details on experimental equipment and procedures are described by Jacobsen et al. (1983).

A frequency range as broad as possible is covered. Then the Kramers-Kronig relations, valid for linear, causal and local response functions may be employed to extract information on the complex dielectric function, $\tilde{\varepsilon}(\omega)$. From the power reflectance, $R(\omega)$, it is possible to calculate the phase shift on reflection, $\theta(\omega)$:

$$\theta(\omega) = \frac{\omega}{\pi} \, P \int_0^\infty \frac{\ln R(\omega')}{\omega^2 - \omega'^2} \, d\omega', \tag{1}$$

and then

$$\tilde{\varepsilon}(\omega) = \left(\frac{1 + \sqrt{R(\omega)}\, e^{i\theta(\omega)}}{1 - \sqrt{R(\omega)}\, e^{i\theta(\omega)}} \right)^2. \tag{2}$$

Table II. Characteristics of some organic conductors. The third column gives high/low temperature character
(M = metal, S = semiconductor, SM = semimetal, SC = superconductor, I = insulator).

Material	σ_{dc}(300K) S cm^{-1}	Character	ϱ	Structure
TTF-TCNQ	600	M/S	0.55	monoclinic
	Cohen et al. (1974)		Kagoshima et al. (1976)	Kistenmacher et al. (1974)
TSF-TCNQ	800	M/S	0.63	monoclinic
	Etemad et al. (1975)		Weyl et al. (1976)	Etemad et al. (1975)
TMTSF-TCNQ	1000	M/S	0.57	triclinic
	Jacobsen et al. (1978)		Pouget (1981)	Bechgaard et al. (1977)
TMTTFF	120	M/S	–	triclinic
-DMTCNQ	Jacobsen et al. (1978)			Jacobsen et al. (1978)
TMTSF	500	M/S	0.50	triclinic
-DMTCNQ	Jacobsen et al. (1978)		Pouget (1981)	Andersen et al. (1978)
HMTTF-TCNQ	400	M/S	0.72	orthorhombic
	Greene et al. (1976)		Megtert et al. (1978)	Greene et al. (1976)
HMTSF-TCNQ	2000	M/SM	0.74	orthorhombic
	Bloch et al. (1975)		Weyl et al. (1976)	Phillips et al. (1976)
DBTTF	40	S/I	0.56	triclinic
-$TCNQC1_2$	Jacobsen et al. (1980)		Mortensen et al. (1983)	Soling et al. (1981a)
HMTSF-TNAP	2400	M/SM	0.58	triclinic
	Bechgaard et al. (1978)		Pouget (1984)	Kistenmacher (1978)
DBTSF	0.0001	S/I	1.0	monoclinic
-$TCNQF_4$	Bryden et al. (1984)		Bryden et al. (1984)	Bryden et al. (1984)
MEM-$TCNQ_2$	0.001	S/I	0.5	triclinic
	Huizinga et al. (1979)			Bosch and v.Bodegom (1977)
$TMTSF_2PF_6$,	500	M/S	0.5	triclinic
-AsF_6,-SbF_6	Bechgaard et al. (1980)			Thorup et al. (1981)
				Soling et al. (1981b)
$TMTSF_2ClO_4$	700	M/SC	0.5	triclinic
	Bechgaard et al. (1981a)			Bechgaard et al. (1981b)
$TMTTF_2Br$	260	M/I	0.5	triclinic
	Delhaes et al. (1979)			Liautard et al. (1982)
$TMTTF_2PF_6$	20	S/I	0.5	triclinic
	Delhaes et al. (1979)			Liautard et al. (1982)
$(BEDT\text{-}TTF)_2I_3$	30	M/SC	0.5	triclinic
	Yagubskii et al. (1984)			Kaminskii et al. (1984)

P denotes principal value. Clearly in Eq. (1) suitable extrapolations for the ranges not covered must be adopted (see, for example, Wooten (1972)). However, if the measured range is sufficiently wide, $\tilde{\varepsilon}(\omega)$ is not very dependent on the particular choice of extrapolations.

For conducting substances, the imaginary part of $\tilde{\varepsilon}(\omega)$ diverges as $\omega \rightarrow 0+$. Hence it is more convenient to introduce the real dielectric function, $\varepsilon(\omega)$, and the frequency dependent conductivity, $\sigma(\omega)$, related to $\tilde{\varepsilon}(\omega)$ by

$$\tilde{\varepsilon}(\omega) = \varepsilon(\omega) + i\sigma(\omega)/\varepsilon_o\omega. \tag{3}$$

It is noted that the area under the $\sigma(\omega)$ curve in a natural way corresponds to the optical oscillator strength. For example, integrating over all frequencies yields the sum rule (Wooten, 1972),

$$\int_0^\infty \sigma(\omega)d\omega = (\pi/2)Ne^2/m, \tag{4}$$

where N is the total electron density and m is the electron mass. As demonstrated later, similar sum rules may with some care be applied to limited frequency ranges and particular groups of electrons.

Basic interactions and instabilities

This section introduces important physical parameters and models, which will be referred to later. Theoretical expectations to the IR properties associated with the models are discussed. Finally, we review shortly the different types of low-dimensional instabilities.

One-electron model

The simplest model for the molecular chain compounds assumes non-interacting electrons, which can move only in the chain direction:

$$H = \sum_{i,\sigma} E_o n_{i,\sigma} - \sum_{i,\sigma} t(c^+_{i,\sigma}c_{i+1,\sigma} + c^+_{i+1,\sigma}c_{i,\sigma}). \tag{5}$$

$c^+_{i,\sigma}$ creates an electron of spin projection σ on site i, and $n_{i,\sigma} = c^+_{i,\sigma}c_{i,\sigma}$ is the occupation number. E_o is the solid state ionization potential, and t is the transfer integral associated with the finite overlap between near neighbour orbitals. More distant overlaps may be safely ignored in molecular crystals. This tight-binding approximation leads to a cosine energy band:

$$\varepsilon_k = E_o - 2t\cos kd, \tag{6}$$

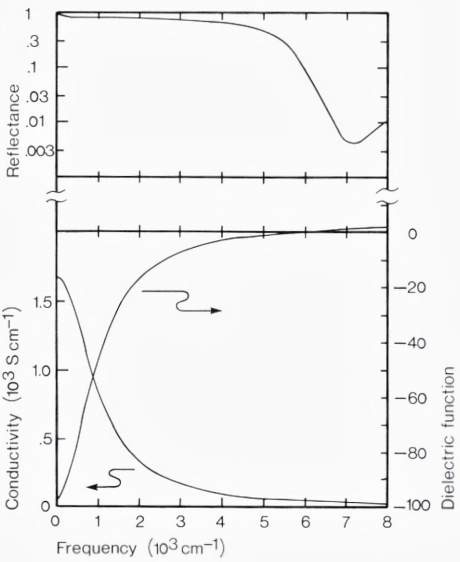

Fig. 3. Optical properties of the Drude model. Notice the logarithmic reflectance scale. Parameters: $\varepsilon_c = 3.0$, $\omega_p = 10000\ cm^{-1}$, $\gamma_{opt} = 1000\ cm^{-1}$.

where d is the molecular repeat distance. With ϱ electrons per site, the band is filled to $\pm k_F = \pm\pi\varrho/2d$ (assuming $t > 0$). Thus the Fermi surface consists of the two parallel planes $k = \pm k_F$. The density of states at the Fermi level is $N(\varepsilon_F) = (\pi t \sin(\pi\varrho/2))^{-1}$.

The IR properties associated with Eq. (5) may be derived in the self-consistent field approximation (see, for example, Wooten (1972)). Assuming a frequency independent relaxation rate, γ_{opt}, and a background dielectric constant arising from virtual high frequency transitions, ε_c, the result is of the Drude form,

$$\tilde{\varepsilon}(\omega) = \varepsilon_c - \omega_p^2/\omega(\omega + i\gamma_{opt}), \tag{7}$$

where the plasma frequency, ω_p, may be calculated from

$$\omega_p^2 = (e^2/\varepsilon_o\hbar^2) \sum_{BZ} f(\varepsilon_k)\partial^2\varepsilon_k/\partial k^2. \tag{8}$$

$f(\varepsilon_k)$ is the Fermi-Dirac occupation number, and the derivative $\partial^2\varepsilon_k/\partial k^2$ is to be taken along the direction of the electric field.

In the present quasi-1D model, Eq. (8) yields

$$\omega_p^2 = 4td^2e^2\sin(\pi\varrho/2)/\pi\varepsilon_o\hbar^2V_m, \tag{9}$$

where V_m is the crystal volume per molecule. This expression is derived for $T = 0$. The explicit temperature dependence may be ignored when $k_BT << \varepsilon_F$, a condition which is normally fulfilled. In Fig. 3 the IR

properties of the Drude model are shown for typical values of the parameters.

Especially noteworthy is the characteristic drop in reflectance in the near IR, which arises from the zero-crossing of $\varepsilon(\omega)$. This is also the frequency of the plasmons, i.e. long wavelength oscillations in the conduction electron charge density. Since the plasmons are longitudinal excitations, they are not optically excitable in a normal incidence experiment, but the sharp drop in reflectance, the plasma edge, is a signature of their existence.

Another point is that the area below the $\sigma(\omega)$ curve is related to ω_p by a partial sum rule

$$\int_{\text{intraband}} \sigma(\omega)d\omega = (\pi/2)\varepsilon_o\omega_p^2. \tag{10}$$

Interchain hopping may easily be incorporated into the model. If, for simplicity, we consider an orthorhombic, 2D model with transfer integrals $t_{\parallel}$ and $t_{\perp}$, the band dispersion is given by:

$$\varepsilon_{\vec{k}} = E_o - 2t_{\parallel}\cos(k_{\parallel}d_{\parallel}) - 2t_{\perp}\cos(k_{\perp}d_{\perp}). \tag{11}$$

Here $d_{\perp}$ is the chain spacing. A small $t_{\perp} << t_{\parallel}$ will introduce a warping of the Fermi surface. For considerable interchain coupling, $t_{\perp} \sim t_{\parallel}$, the Fermi surface will be closed, cylindrical.

From Eqs. (8) and (11) a tensorial $\overline{\overline{\varepsilon}}$ may be calculated. By symmetry the principal axes are the chosen directions, along which Drude behaviour is found with plasma frequencies that in the general case must be calculated numerically. As an example to be used later we show in Fig. 4 the normalized plasma frequencies for a quarter-filled band. The crossover from open to closed Fermi surface is indicated.

Electron-phonon coupling

In molecular crystals there are many possible sources to the electron-phonon coupling. Usually, the most important are considered to be: (1) Modulation of t by external modes (acoustic translational and rotational modes), and (2) modulation of E_o by internal modes (molecular vibrations). A good discussion, including estimates for TTF-TCNQ, has been given by Conwell (1980). The second source to the electron-phonon interaction is of central interest to analysis of IR spectra, since the molecular vibration frequencies span the IR range (100-3000 cm^{-1}).

The origin of the electron-molecular vibration (emv) coupling is easily understood. The conduction electron orbital energy is in general a func-

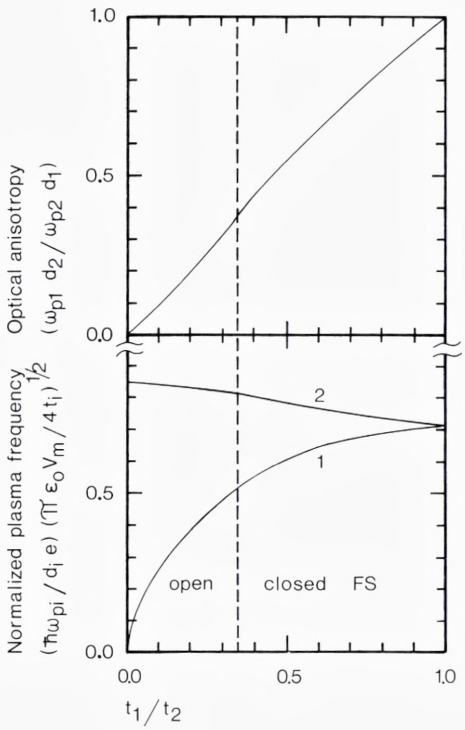

Fig. 4. Anisotropic plasma behaviour in 2D orthorhombic and quarter-filled tight-binding model. The dashed line indicates the cross-over from open (left) to closed (right) Fermi surface. The bottom graphs show normalized plasma frequencies.

tion of the exact atomic configuration in the molecule. Hence the molecular vibrations will modulate the one-electron energies, giving rise to the emv coupling. For a non-degenerate level only the totally symmetric A_g-modes couple linearly to the electrons (Duke et al., 1975). The A_g-modes are Raman active, but IR inactive. However, when charge can move to and from the molecule as in the solid state or in molecular complexes in solution, the modes may, through the emv coupling, borrow oscillator strength from the conduction electrons and give rise to spectacular effects in the IR (see, for example, Bozio and Pecile (1980) and references therein). If the electronic structure is sufficiently simple, information on coupling constants may be extracted from the spectra. One example is the material MEM-$TCNQ_2$ at 300K, where the TCNQ molecules are organized in stacks as quasi-isolated dimers, with one electron per dimer. In Fig. 5 is shown the IR spectra. Note the strong features in the chain axis spectrum, which has been used to obtain the emv coupling constants for TCNQ (Rice et al., 1980). The coupling constants may also be calculated theoretically and reliable values are now known for several molecules.

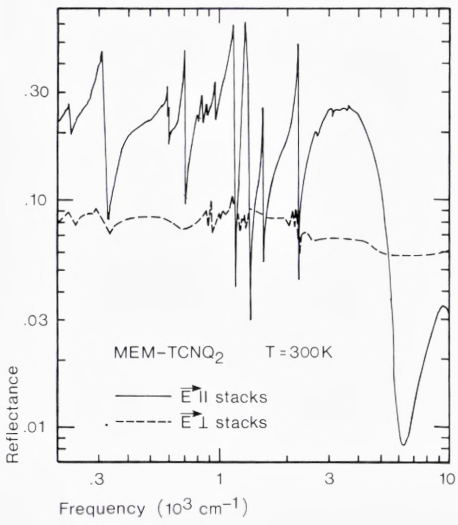

Fig. 5. Polarized reflectance of MEM-$TCNQ_2$ at 300K. Notice the logarithmic scales. (Rice et al., 1980).

In the organic conductor with uniform stacks, the emv coupling should not have direct resonant effects on the optical spectra. Resonances/antiresonances are only activated if the symmetry is broken, either by structural distortion or by the presence of charge-density waves (CDWs) in the system.

Assuming unbroken symmetry, the question arises how electron-phonon interactions influence the IR behaviour. The main deviations from the Drude spectrum are found in the pure metal at low temperature, where the electron-phonon coupling does not contribute to the dc-resistivity. Then the dc-relaxation rate, γ_{dc}, is determined by residual impurities and defects, and a near δ-function contribution to $\sigma(\omega)$ is obtained. As ω is increased and reaches frequencies of current-degrading phonons, photon absorption assisted by phonon emission becomes possible and a threshold in $\sigma(\omega)$ is anticipated (Holstein (1954, 1964); see also Allen (1971)). At frequencies well above all important phonon frequencies, the relaxation rate $\gamma_{opt} \rightarrow \pi\lambda_{tr}<\omega_{ph}>$, where λ_{tr} is an appropriate dimensionless electron-phonon coupling constant and $<\omega_{ph}>$ is an average phonon frequency. In terms of oscillator strength, a fraction $\sim\lambda_{tr}/(1+\lambda_{tr})$ of the low frequency Drude contribution appears as IR absorption with a high frequency Drude tail determined by phonon emission processes. However, the sum rule, Eq. (10), is still expected to be obeyed.

At high temperatures $k_BT >> \hbar<\omega_{ph}>$, and both phonon absorption

and emission contributes to γ so $\gamma_{dc} \simeq \gamma_{opt}$ and a single Drude absorption is found. We note that in the molecular metals the high temperature limit is never reached with respect to the majority of the vibrational modes. Thus Holstein thresholds may be encountered, even at room temperature.

Electron-electron interactions

The electron-electron Coulomb interaction is more difficult to deal with. It is commonly assumed that it can be treated as in ordinary metals. Thus the long range interaction part is frozen in the zero point motion of the plasmons, while the short range part gives rise to quasiparticles with screened interactions (see, for example, Pines (1964)). The screening efficiency was recently discussed by Mazumdar and Bloch (1983). Their conclusions may be described as follows: Only on-site and nearest neighbour interactions need to be considered. Thus the proper model Hamiltonian is of the extended Hubbard type (Hubbard, 1978):

$$H = \sum_{i,\sigma} E_o n_{i,\sigma} - \sum_{i,\sigma} t(c^+_{i,\sigma}c_{i+1,\sigma} + c^+_{i+1,\sigma}c_{i,\sigma}) + \sum_i U n_{i\uparrow} n_{i\downarrow} + \sum_{i,\sigma,\sigma'} V n_{i,\sigma} n_{i+1,\sigma'}. \quad (12)$$

U is the extra electrostatic energy associated with two carriers on the same site, and V is the corresponding energy for two carriers on neighbour sites. Both U and V are to be considered effective, screened values, which depend strongly on band filling (ϱ). For $\varrho = 0.5$ and 1.0 the screening is found to be inefficient ($U > 4t$). In the intermediate range, screening may be quite efficient ($U << 4t$), mostly so for $\varrho \simeq 0.7$-0.8. $\varrho = 1$ (half-filled band) constitutes a special case, since for any finite U, there is a gap in the excitation spectrum (Lieb and Wu, 1968). Thus the 1D half-filled band is an insulator of the Mott type. For $\varrho < 1$ there is no clear evidence for a gap in the energy spectrum of Eq. (12).

We now turn to the IR properties of a system described by the Hubbard model. First we note the existence of a modified partial sum rule for the intraband absorption (Maldague, 1977):

$$\int_{\text{intraband}} \sigma(\omega)d\omega = -(\pi e^2 d^2/2\varepsilon_o)\langle H_t \rangle \quad (13)$$

$\langle H_t \rangle$ is the ground state expectation value of the transfer terms of H. Since H_t determines the ground state in the absence of correlation effects, it is evident that finite correlation reduces the oscillator strength below that of Eq. (10).

The next issue is the distribution of oscillator strength. Again $\varrho = 1$ is a special case. Even in the weak coupling limit, $U << 4t$, optical absorption may occur via Umklapp electron-electron scattering. In the strong coupling limit, $U >> 4t$ ($V=0$) Lyo and Gallinar (1977) find a symmetric absorption extending from $U-4t$ to $U+4t$. The oscillator strength is proportional to t^2/U. A finite nearest neighbour interaction induces an asymmetry in the absorption (Lyo, 1978). Then there is a strong onset of absorption at $U-4t$ and a tail extending to $U+4t$. Physically the absorption band corresponds to charge transfer transitions into states with doubly occupied sites.

For $\varrho < 1$, the main question is whether the dominant part of the oscillator strength goes into charge transfer bands of the correlation type ($\hbar\omega \sim U,V$) or whether it appears in a low frequency Drude-like absorption. The answer again depends on the band-filling. However, there is strong evidence from various approximative calculations (Maldague, 1977) and finite chain calculations that for $0.5 < \varrho < 0.6$ less than 10% of the oscillator strength appears in correlation bands.

Finally, it is of some interest to describe a specific limit of Eq. (12): $V = 0$ and $U \to \infty$ (double occupancy of sites excluded). In this case the translational and the spin degrees of freedom are decoupled (Sokoloff, 1970). The spin susceptibility is Curie-like and the electrons behave otherwise as a system of non-interacting spinless fermions described by the usual tight-binding model of Eq. (5,6). Because of the spinlessness the density of states is halved and the band is now filled to $k = \pm\pi\varrho/d$. The optical properties are Drude-like, as described above, and the relative reduction of oscillator strength is obtained from Eq. (9):

$$\int_{U\to\infty} \sigma(\omega)d\omega \Big/ \int_{U=0} \sigma(\omega)d\omega = \cos(\pi\varrho/2). \tag{14}$$

It is noted that with respect to oscillator strength, the dense electron system is more sensitive to the high U limit than the less dense system.

Low-dimensional instabilities

The linear chain structure of the molecular conductors has important consequencies for the occurrence and behaviour of instabilities. As discussed below the quasi-one-dimensionality leads to phase transitions not known in isotropic systems. At the same time thermodynamic fluctuations tend to suppress the phase transition temperatures. It is well-known that long range order cannot persist in a 1D system for $T > 0$. Thus usually short range order develops below some scale temperature,

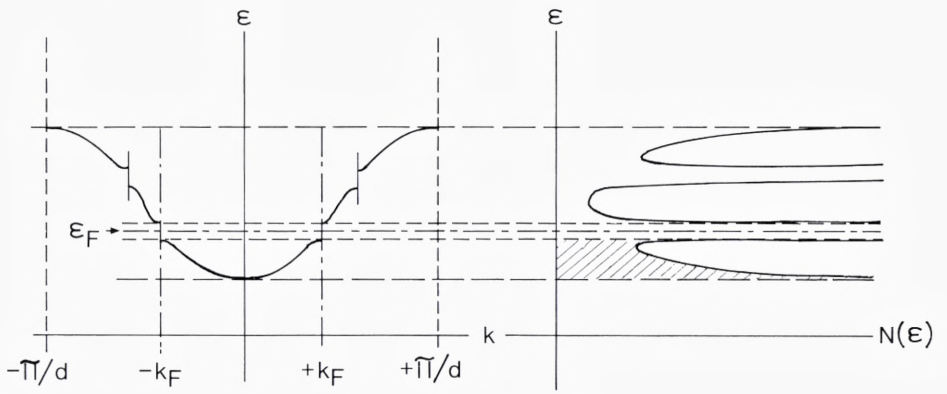

Fig. 6. Effect of $2k_F$-distortion on cosine band and density of states.

T_{MF}. As temperature is lowered, the on-chain correlation length grows and since the real systems consist of arrays of chains any finite interchain coupling will eventually induce long range 3D order at a temperature, T_C, which defines a three-dimensional phase transition. In the range $T_C < T < T_{MF}$, the fluctuations may have important impact on the physical properties.

The most famous of the 1D instabilities is that of the linear chain metal. We shall here repeat the argument by Peierls (1955) with reference to Fig. 6. The figure shows the band structure and density of states of Eq. (6) with the inclusion of a weak $2k_F$-potential which spans the Fermi sea. The crucial point is that this potential opens a gap at the Fermi level, ε_F, and thus lowers the energies of those electrons closest to ε_F. Due to the 1D divergent density of states near a gap this energy gain will always outweigh the cost of creating the $2k_F$-potential. The latter arises from a CDW/periodic lattice distortion mediated by the electron-phonon coupling. For a half-filled band a detailed calculation gives the following zero temperature gap (Rice and Strässler, 1973):

$$E_g = 2\Delta = 2\varepsilon_F/\sinh(1/\lambda\text{-}\ln 2) \simeq 8\varepsilon_F \exp(-1/\lambda). \tag{15}$$

The last expression applies for $\lambda << 1$. The dimensionless electron-phonon coupling constant, λ, is related to the bare coupling constant, g, the density of states in the metallic state, $N(\varepsilon_F)$, and the unperturbed phonon frequency, ω_{2k_F}, by

$$\lambda = g^2 N(\varepsilon_F)/\hbar\omega_{2k_F}. \tag{16}$$

The temperature dependence of the gap is BCS-like (Bardeen et al., 1957). Thus the mean field scale temperature, where the gap vanishes is given by

$$k_B T_{MF} = 2\Delta/3.52. \tag{17}$$

The actual phase transition temperature, T_C, may be fluctuation suppressed below T_{MF}.

There are two kinds of elementary excitations associated with the Peierls state: (1) Electron-hole excitations across the gap and (2) phase and amplitude oscillations of the $2k_F$-CDW. The phase oscillations have a dipole moment and are thus IR active. Fröhlich (1954) noted that in situations where the energy of the CDW is independent of the phase, the CDW is free to move through the crystal and carry current in a way reminiscent of superconductivity. In real systems this may happen in incommensurate cases (where λ_{2k_F} does not match the lattice) for $T \geqslant T_C$, where, however, a finite correlation length will limit the conductivity. For $T < T_c$ the CDW is pinned and appears as a far IR absorption.

Rice and coworkers (Rice et al. (1975), Rice (1978)) have emphasized the role of simultaneous involvement of many phonons. They find that for the molecular conductors, it is to be expected that much of the Peierls gap is due to the sizeable number of intramolecular modes coupled to the electrons, while the dynamic properties, e.g. effective mass, of the CDW is dominated by the low frequency external modes. The CDW is a complicated superposition of contributions from each mode. In the infrared spectrum phase oscillations may be identified in the vicinity of each unperturbed mode frequency (Rice et al., 1977). This is a good example of IR-activation of the A_g-modes.

A number of other instabilities have close analogies to the Peierls instability. The Overhauser instability (Overhauser, 1960) may occur when the electron-phonon interaction is comparatively weak and a finite short range electron-electron interaction is present. Then a $2k_F$ spin-density wave will act on the electrons as an effective $2k_F$-potential through the modulation of the exchange interaction (Slater, 1951). The energetics are then similar to what is described above, but the effective coupling constant rather is $N(\varepsilon_F)\tilde{U}$, $\tilde{U}$ being an appropriate Coulomb interaction.

Another important modification of the Peierls instability happens in the limit of strong electron-electron interaction, where we may let $U \rightarrow \infty$. As stated above, the translational degrees of freedom are described in terms of non-interacting spinless fermions in a tight-binding band filled

to $\pm 2k_F$. The fermion-phonon interaction is of the same form as that entering the theory for the Peierls instability, thus a $4k_F$-CDW Peierls type of instability may occur (Bernasconi et al., 1975). The behaviour is completely analogous if the differences in wavenumber, in band-filling, and in dimensionless coupling constant are taken into account.

If the electrons are locked into such a $4k_F$-CDW or are localized by direct Coulomb interaction (Mott insulator) the magnetic subsystem is susceptible to yet another $2k_F$-instability, the spin-Peierls instability (Chesnut, 1966), which is a magnetic analogue. In this case the coupling between the antiferromagnetic exchange integral, J, and the phonons induces a $2k_F$ modulation of J, which quenches the magnetic susceptibility.

After this short discussion we stress that for the instabilities to occur, the 1D nature is crucial. The Peierls type instability depends on the ability of a single wavevector to nest the entire Fermi surface. The nesting efficiency will in general deteriorate as interchain coupling increases (see, for example, Horovitz et al. (1975)), but even 3D materials may undergo density wave formation if segments of the Fermi surface allow nesting.

As a last remark it is noted that also superconductivity may occur in 1D systems. However, it is not clear at present how one may distinguish between a quasi-1D superconductor and a highly anisotropic 3D superconductor.

Plasma edges and band structure

Measurements of the polarized reflectance in the vicinity of the plasma edge have frequently been used to obtain estimates for the transfer integrals. The method consists of fitting a reflectance model based on the Drude expression of Eq. (7) to the data in a limited range and then use Eq. (8) in conjunction with information on carrier density and crystallographic data to derive values for t. Such an approach has often been criticized (see, for example, Williams and Bloch (1974)) because the molecular conductors show strong deviations from Drude behaviour at lower frequencies (cfr. next section). The aim of the present section is to use experimental data in arguing for the validity of the Drude analysis. The underlying idea is that the plasma edge is a signature for existence of plasmons. Since these are long wavelength oscillations in the charge density their frequency is intuitively expected to be insensitive to the

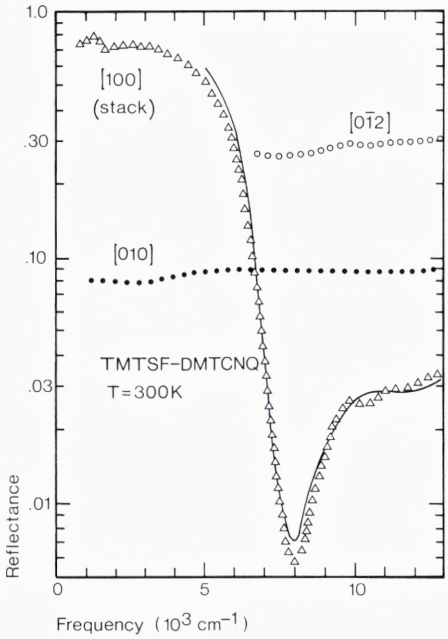

Fig. 7. Polarized reflectance of TMTSF-DMTCNQ at 300K. Notice the logarithmic reflectance scale. The solid line is a fit of the Drude model to the chain axis spectrum. An extra oscillator has been added to the model to account for the absorption band near 10000 cm^{-1}.

details in the short range interactions, which give rise to the non-Drude features observed in the infrared. Thus the Drude expression should be viewed as a convenient mathematical tool in estimating the plasmon frequency, Ω_p, and the background dielectric constant, ε_c. Then the transfer integral is calculated from the unscreened plasma frequency, $\omega_p \simeq \Omega_p \sqrt{\varepsilon_c}$.

During the argumentation we shall further attempt a decomposition of average transfer integrals in double-stack conductors and show examples of materials with 2D character.

Chain axis

As a typical example we present in Fig. 7 the polarized room temperature reflectance of TMTSF-DMTCNQ with a model fit to the chain axis spectrum. The most striking feature is the well-developed plasma edge observed along the stacks. Virtually no dispersion is seen in the other directions. The infrared spectra are indeed a remarkable manifestation of the linear chain structure.

The plasma edge is quite sharp with a drop in reflectance of more than two orders of magnitude. This hints to the existence of rather well-defined plasmons, i.e. $\varepsilon_1 = 0$ and $\varepsilon_2 << 1$ are simultaneously obeyed.

Plasmons have so far been observed directly in TTF-TCNQ only (Ritsko et al., 1975). In that case the plasmon frequency is in complete agreement with the optical properties (Tanner et al., 1976).

The solid line is a fit of a model based on the Drude expression, Eq. (7), with an extra oscillator added. The latter takes into account the absorption band near 10000 cm^{-1}, which is observed in all TCNQ based materials and which is presumably intramolecular in origin (Tanaka et al., 1978).

A close inspection of the quality of the fit reveals a systematic deviation from the Drude model in the edge region. The data points fall below the model both at low frequencies (entering the IR) and near the minimum. The model could be improved by allowing the relaxation rate, γ_{opt}, to decrease slowly with frequency in the near infrared range. This observation, which is made in many of the organic conductors leads us to shortly discuss the origin of optical absorption in the near IR. Usually the absorption is attributed to phonon assisted electron-hole excitations within the one-electron tight-binding band. However, the bandwidth, 4t, is found to be of order 0.7-1.0 eV corresponding to frequencies of 6000-8000 cm^{-1}. But as the frequency exceeds the bandwidth many phonon assisted processes become impossible by energy conservation. For $\hbar\omega > 4t$ only processes involving emission of high energy phonons are conceivable. Thus such absorption mechanisms in a natural way account for the observed frequency dependence of γ_{opt}. This discussion viewed together with the remarks made on the Holstein mechanism previously, strongly suggests that the near IR relaxation rate has little to do with the low frequency scattering, which governs the static conductivity. Indeed, the temperature dependence of γ_{opt} is much weaker than that of the dc-conductivity in most cases (see, for example, Bright et al. (1974)).

In Table III is presented the results of Drude analysis and transfer integral calculation for a number of materials, in all cases for the stacking direction, using Eq. (9). For the double-stack conductors the value given is the average of donor and acceptor bandwidths. For the single-stack conductors the slight dimerisation is neglected.

Since the table contains some results for single- and double-stack conductors with the same molecule, it should be possible to decompose the bandwidth of the double-stack conductors into donor and acceptor contributions adopting certain assumptions. For this purpose interplanar distances (ipd) for the molecules in the stacks have been included. Our principal assumptions are, (1) that the bandwidth depends only on the

Table III. Chain axis Drude parameters and bandwidths. Also given are cation and anion interplanar distances.

Material	T K	ε_c	γ cm^{-1}	ω_p cm^{-1}	$4\bar{t}$ eV	cation ipd Å	anion ipd Å
TTF-TCNQ	300	3.27	1430	11400	0.61	3.48	3.17
TSF-TCNQ[a]	300	–	–	12200	0.69	3.52	3.21
TMTSF-TCNQ[a]	300	–	–	12000	0.89	3.59	3.26
TMTTF-DMTCNQ[a,b]	300	–	–	10700	0.77	–	–
TMTSF-DMTCNQ	300	2.91	1180	11200	0.88	3.64	3.31
HMTTF-TCNQ	300	3.15	1260	12400	0.78	3.57	3.23
HMTSF-TCNQ	300	3.30	1030	14200	1.03	3.6	3.2
DBTTF-$TCNQCl_2$	300	2.51	2000	7500	0.41	3.51	3.41
HMTSF-TNAP	300	2.95	1100	11300	0.84	3.58	3.28
$TMTTF_2PF_6$	300	2.50	1380	8900	0.80	3.58	–
$TMTSF_2AsF_6$	300	2.56	1230	9900	1.00	3.63	–
–	30	2.55	1160	10500	1.11	–	–

[a] estimate from edge shift

[b] ϱ is assumed equal to 0.5 (as in the isostructural TMTSF-DMTCNQ)

molecular species and ipd, and (2) that t increases ~5% for a decrease in ipd of 1%. The first assumption is based on the quasi-1D nature of the materials and on the very similar overlap patterns observed for the same molecule in different materials (see references of Table II). The second assumption is based on molecular orbital calculations (Herman, 1977) and on the change in t observed on cooling to low temperatures. This change usually amounts to +10% (Table III), while the stack-contraction is about 2% (Schultz et al., 1976).

The resulting decomposition is given in Table IV. There is a rather large spread in bandwidths from 0.4 to 1.3 eV. Substituting Se for S in TTF-based molecules always results in increases in t as expected from the increased overlap. It is noteworthy that methylation of TTF-based molecules leads to strong increases in bandwidths (Jacobsen et al., 1983). Although we cannot go into a detailed discussion of the results in context of other physical properties the general trends are clearly consistent with independent knowledge. We give four specific examples: (1) The thermoelectric power of TMTSF single stack materials yields a bandwidth slightly larger than 1 eV (Mortensen, 1982). (2) HMTSF-based metals have exceptionally high conductivities (cfr. Table II). (3) The thermoelectric power of TTF-TCNQ is large and negative while it is close to zero for TSF-TCNQ (Chaikin et al., 1976). (4) The conductivity of

TMTSF-TCNQ is significantly higher than that of TSF-TCNQ (Table II).

Another argument for the validity of the present approach is the agreement in values for the DMTCNQ-bandwidths. The number obtained for TMTTF-DMTCNQ is based on analysis of data for the single-stack compound $TMTTF_2PF_6$, which is a semiconductor with strong non-Drude behaviour in the IR (Jacobsen et al., 1983), while the number for the selenium analogue is based on data for an excellent metal, $TMTSF_2AsF_6$, which is close to Drude behaviour in the IR.

A final direct demonstration of the main point i.e. the simple connection between one-electron bandwidth and plasmon frequency will be given next while discussing 2D compounds.

Interchain contact

There are at present two groups of organic conductors, which show considerable interchain coupling. They are both of single-stack type with donor molecules, $\varrho = 0.5$, and inorganic counterions. The basic structural features are also the same: Sheets of molecular stacks interchanging with layers of counterions. The important interchain contact is *in* the sheets so that the materials are effectively two-dimensional. Interestingly these materials among them count the only representatives of organic superconductivity so far.

Table IV. Single-stack bandwidths. T = 300K

Donor		Acceptor	
Stack	4t eV	Stack	4t eV
TTF-(TCNQ)	0.41	(TTF)-TCNQ	0.81
TSF-(TCNQ)	0.62	(TSF)-TCNQ	0.76
TMTSF-(TCNQ)	1.06	(TMTSF)-TCNQ	0.70
TMTTF-(DMTCNQ)	0.80	(TMTTF)-DMTCNQ	0.74
TMTSF-(DMTCNQ)	0.93	(TMTSF)-DMTCNQ	0.70
HMTTF-(TCNQ)	0.80	(HMTTF)-TCNQ	0.76
HMTSF-(TCNQ)	1.3	(HMTSF)-TCNQ	0.76
HMTSF-(TNAP)	1.3	(HMTSF)-TNAP	0.4

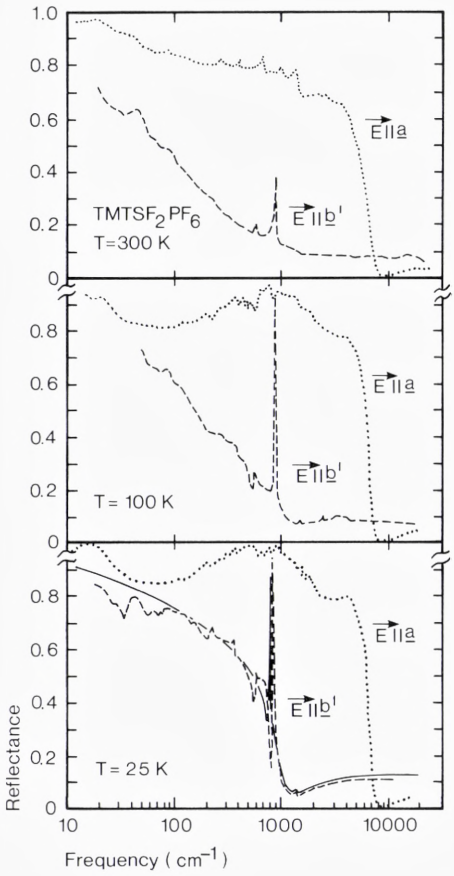

Fig. 8. Polarized reflectance of $TMTSF_2PF_6$ at 300K, 100K, and 25K. Notice the logarithmic frequency scale. The chain axis is along a. The solid line is a Drude fit to the low temperature spectrum with polarization perpendicular to the chains. One extra oscillator has been added to the model to account for the sharp vibrational line near 800 cm^{-1}. (Jacobsen et al. 1981).

Their actual anisotropy may be deduced from reflectance studies. As an example from the $TMTSF_2X$-family we present in Fig. 8 the polarized reflectance of $TMTSF_2PF_6$ at three temperatures: 300K, 100K and 25K (Jacobsen et al., 1981). It is evident that a reasonably well-defined plasma edge appears in the *b'*-direction at low temperature. The *b'*-direction is perpendicular to the stacks in the sheets of TMTSF-molecules. Most of the sharp lines superimposed on the edge arise from normal IR active modes in PF_6^-. The transverse reflectance edge appears at a frequency about ten times lower than that of the stacking axis edge. A Drude analysis may be performed (solid line) and the ratio $(\omega_{pb'}/\omega_{pa'})$ (a'/b') which refers to the model of Fig. 4 is 0.09. Calculation yields $t_{b'} \simeq 22$ meV, about 10 times smaller than t_a. Although $t_{b'}$ is significant as compared to k_BT for all temperatures of interest the Fermi surface must clearly be open. Table V gives Drude parameters and transfer integrals

Table V. Drude parameters, transfer integrals, and b-axis lattice constants in $(TMTSF)_2X$, $\vec{E}||b'$

X	ε_c	ω_p cm^{-1}	γ cm^{-1}	$t_{b'}$ meV	b Å
ClO_4^-	3.5	2020	250	24	7.678
SbF_6^-	3.5	1510	300	18	7.728
AsF_6^-	3.5	1670	350	20	7.711
PF_6^-	3.5	1830	500	22	7.711

for several members of the $TMTSF_2X$ family (Jacobsen et al., 1983). It should be noted that there is a reasonable correlation between $t_{b'}$ and the b-axis lattice constant. The largest $t_{b'}$ is found in the densely packed $TMTSF_2ClO_4$, the only ambient pressure superconductor in the series. This gives some support to the simple band picture of Yamaji (1985) which predicts a critical value of $t_{b'} \simeq 25$ meV. The values are also in good agreement with results of band structure calculations (Grant, 1983).

The other materials group of interest is based on BEDT-TTF (or ET). The first reported ambient pressure superconductor in this family is triclinic (β-phase) ET_2I_3 (Yagubskii et al., 1984). Fig. 9 shows the polarized reflectance of this material in the *a-b* plane (Jacobsen et al., 1985). Again this plane corresponds to the sheets of molecular stacks. Interestingly, the highest plasma frequency is associated with the direction perpendicular to the chains, while the chain direction shows much weaker metallic character in the infrared properties. Although unusual, such behaviour is consistent with the molecular arrangement in the crystal (Kaminskii et al., 1984) and has also been seen optically at room temperature in several materials from the family (Tajima et al. (1984) and Koch et al. (1985)).

In Table VI we list Drude parameters and estimated transfer integrals for ET_2I_3. Again the results of Fig. 4 have been used. Thus the analysis is based on a simplified orthorhombic model and the transfer integrals given are weighted averages of several transfer integrals in the correct triclinic model. The rather small values of t are consistent with a low room temperature conductivity (~30 Scm^{-1}, isotropic in the *a-b*-plane) and the near isotropy is confirmed by thermopower measurements of Mortensen et al. (1985). The validity of the plasma edge Drude analysis

Table VI. Drude parameters and transfer integrals in β-ET_2I_3.
|| Denotes the chain axis, ⊥ the direction perpendicular to the chains in the *a-b* plane.

axis	T K	ε_c	ω_p cm^{-1}	γ cm^{-1}	<t> eV
||	40	4.0	5740	2270	0.10
⊥	40	3.8	9600	540	0.13
⊥	300	3.8	9100	1360	0.12

is again confirmed. It is particularly interesting to compare the 40K and 300K analysis of the data for the perpendicular direction. It is obvious from Fig. 9 and even more so from the dielectric function reproduced in Fig. 10 that the 300K spectrum is non-Drude in the IR while the 40K spectrum is near-Drude in the entire measured range. Nevertheless, the predicted plasma frequencies are different only by an amount expected

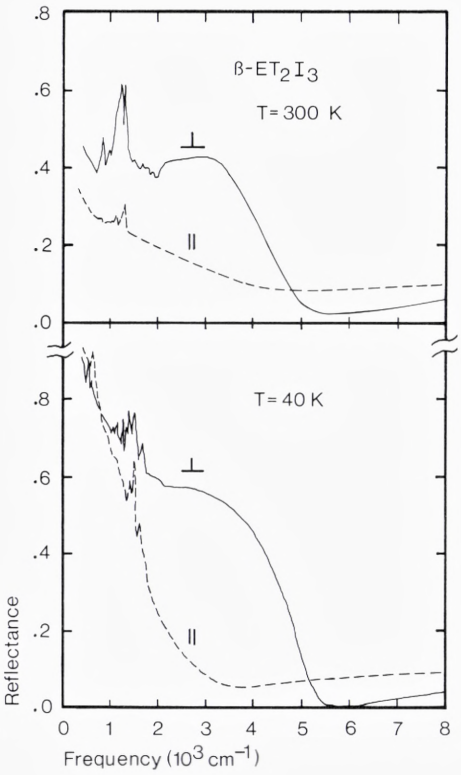

Fig. 9. Polarized reflectance of β-ET_2I_3 at 300K and 40K. The stacking axis is designated ||, while ⊥ refers to a direction perpendicular to the stacks in the a-b plane. (Jacobsen et al., 1985).

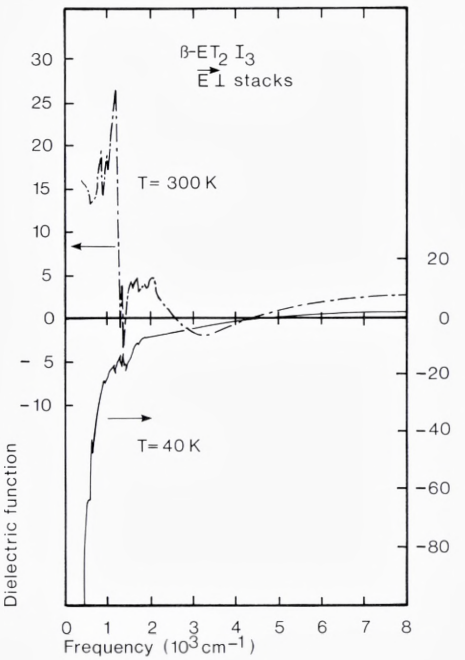

Fig. 10. Real part of $\tilde{\varepsilon}(\omega)$ for β-ET_2I_3 perpendicular to the chains, for T=300K and 40K. Notice the different scales for the two curves. (Jacobsen et al., 1985).

from a thermal contraction induced change in $t_\perp$ (Table VI). This is also evident from Fig. 10 by noting that the zero-crossing in $\varepsilon(\omega)$ near 5000 cm^{-1} only shifts slightly.

Hence our principal conclusion of this section is that careful analysis of reflectance data in the plasmon region yields reliable estimates for transfer integrals. These estimates will be used subsequently while discussing the IR spectra.

Size and distribution of infrared oscillator strength

After having discussed the plasma edge range we now turn to the actual infrared excitation spectra of organic conductors. The aim is to understand the deviations from Drude behaviour in terms of the short range electron-electron and electron-phonon interactions. In Fig. 11 is shown 300K-spectra of 4 double-stack conductors with widely different physical properties (Jacobsen et al., 1984). HMTSF-TNAP, TTF-TCNQ and DBTTF-$TCNQCl_2$ are incommensurate conductors with slightly more than quarter-filled one-electron bands, while DBTSF-$TCNQF_4$ has half-

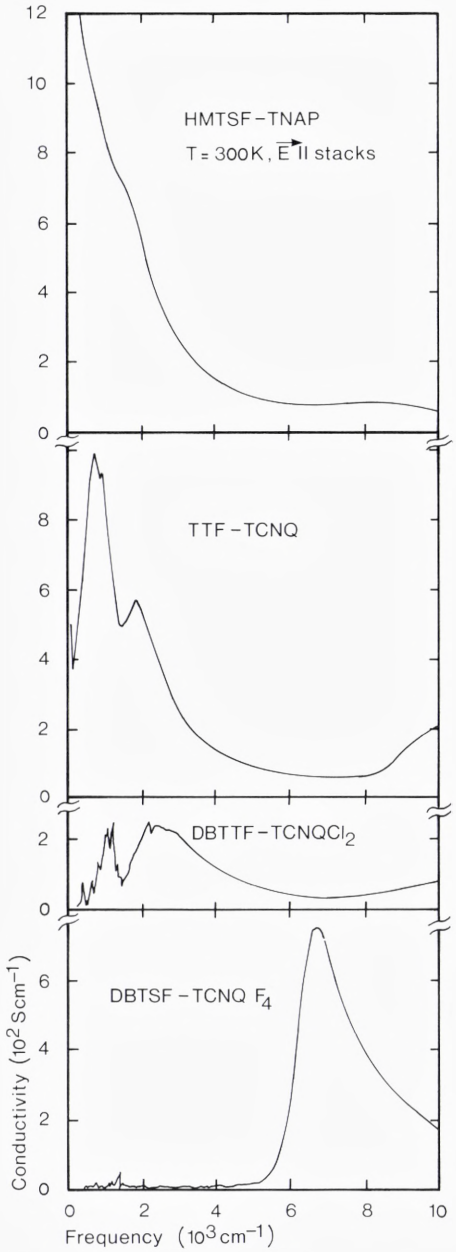

Fig. 11. Frequency dependent conductivities of 4 doublestack conductors at T=300K, along the stacks. (Jacobsen et al., 1984).

filled bands. All materials are expected to be metals in the absence of Coulomb interactions and at 300K there is no evidence for the $2k_F$-distortion, which might destroy the metallic state by pure structural effects.

DBTSF-TCNQF$_4$ is known to be a Mott insulator (Lerstrup et al., 1983), and as we shall shortly discuss, available theory allows a rather unambiguous interpretation of the spectrum.

HMTSF-TNAP is a high conductivity, wide band metal, and the IR behaviour is indeed rather close to Drude behaviour with a monotonic $\sigma(\omega)$. TTF-TCNQ is also a metal but of intermediate bandwidth and with distinct deviations from the Drude spectrum. The oscillator strength is shifted away from zero frequency and fine structure is seen near molecular vibration frequencies. These features are even more pronounced in the narrow band material DBTTF-TCNQCl$_2$, which is a magnetic semiconductor. It is obvious that these room temperature spectra can not be rationalized within traditional 3D models like the Holstein absorption picture.

In the following we first derive parameters for the Mott insulator case. Next we review the physical properties of DBTTF-TCNQCl$_2$ and argue for using the simple $U \rightarrow \infty$ model for this material. Then the size of the IR oscillator strength for a number of organic conductors is compared with expectations based on bandwidth estimates. It is suggested that Coulomb correlations modify the wavefunctions appreciably in all materials. However, depending on band-filling and dimensionality the effect on other physical properties differs widely. Finally, we discuss the temperature dependent IR properties of TTF-TCNQ with special emphasis on understanding the separate roles of the two chains.

The Mott insulator ($\varrho = 1$)

The frequency dependent conductivity of DBTSF-TCNQF$_4$ resembles surprisingly well the prediction by Lyo (1978) for the extended Hubbard model with half-filled one-electron bands. The absorption is dominated by a charge transfer band corresponding to the creation of a doubly occupied site. A finite near neighbour interaction, V, produces a rather strong onset of absorption at U-4t as observed near 5500 cm^{-1} $\simeq$ 0.7 eV in the present case. Additional information may be obtained from the size of the oscillator strength. It is assumed that it follows that of the isolated Hubbard dimer (Rice, 1979):

$$\int \sigma(\omega)d\omega / \int_{(U=0)} \sigma(\omega)d\omega = (1 + (U/4t)^2)^{-1/2}, \tag{18}$$

(correct for $U/4t << 1$ and $>> 1$ (Lyo, 1978)).

Then we find $U \simeq 1.4$ eV and $4t \simeq 0.7$ eV. Such a value for the bandwidth appears reasonable when compared to the results of Table III

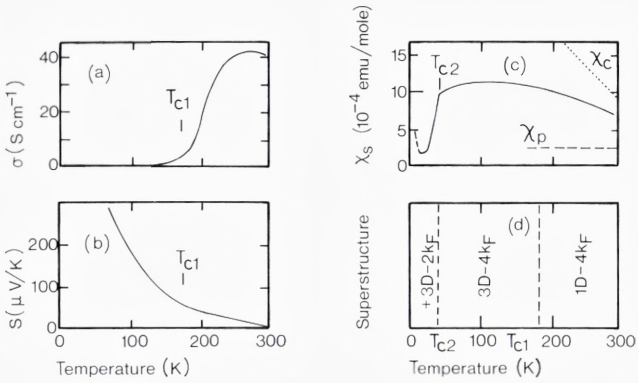

Fig. 12. Basic physical properties of DBTTF-TCNQCl$_2$. See the discussion in the text.

for similarly composed materials (e.g. TSF-TCNQ) but an independent estimate is not available. U/4t $\simeq$ 2 for the half-filled band case is in accord with theoretical expectations (Mazumdar and Bloch, 1983).

As a side-remark it is noted that the A_g-vibrational modes are not activated in the Mott insulator. Charge localization does not suffice: symmetry breaking is a necessary prerequisite for IR activation.

The infinite U model ($\varrho < 1$)

DBTTF-TCNQCl$_2$ is a good example of a non-metallic, but incommensurate (ϱ = 0.56) and near quarter-filled organic conductor. The physical properties are known in rather great detail and are summarized in Fig. 12. The dc conductivity and the thermoelectric power are consistent with the existence of a one-electron gap of order 200-250 meV (1500-2000 cm^{-1}). The activated behaviour is cleanest below T_{c1} = 180K where a slight anomaly is observed. The spin susceptibility, χ_S, is high, about three times the expected non-enhanced Pauli value (χ_P) at 300K, and remains high to T_{c2} = 36K, below which temperature it vanishes rapidly. Note that χ_S (300K) is about $\frac{2}{3}$ of the Curie value (χ_c) for the appropriate carrier density. Finally, diffuse X-ray scattering has shown the existence of rather large amplitude 4k_F-CDWs. Down to T_{c1} there are only weak interchain correlations. T_{c1} is found to be a 3D ordering temperature, while T_{c2} involves the onset of 3D-2k_F scattering.

The implications of these observations are obvious: Enhanced magnetic susceptibility and occurrence of 4k_F-CDWs may both be taken as evidence for important electron-electron correlations. The two transition temperatures also indicate a substantial decoupling of the spin and translational degrees of freedom. The overall behaviour is common to a

larger group of low conductivity materials and the physical picture is the following: The carriers are fairly localized even at high temperature due to the Coulomb repulsion between them. The spins experience a weak antiferromagnetic exchange coupling and through interaction with the lattice undergo a spin-Peierls transition at low temperature. With this discussion we have established that DBTTF-$TCNQCl_2$ is a strongly correlated, incommensurate organic conductor with a sizeable energy gap in the excitation spectrum.

In Fig. 13(a) $\sigma(\omega)$ is shown at 100K. The main difference from the 300K spectrum is a sharpening of the vibrational structure below 1500 cm^{-1}. In both spectra there is a broad maximum around 2000 cm^{-1}, which may be interpreted as arising from a gap in the electronic spectrum in accordance with the low frequency transport properties. This gap, the intensity of the vibrational structure, the presence of $4k_F$-CDWs, and the apparant decoupling of magnetism and electronic behaviour leads us to suggest that DBTTF-$TCNQCl_2$ is subject to an »infinite«-U Peierls instability partly stabilized by the emv coupling. A zero temperature model for $\sigma(\omega)$ of the ordinary $2k_F$ (U=0) Peierls semiconductor has been given by Rice (1978). Because of the formal analogy with this case the theory can be immediately applied, when proper account for the spinlessness of the fermions is taken. As stated earlier the difference concerns the band-filling and the density of states. Rice gives the following expression for $\tilde{\varepsilon}(\omega)$:

$$\tilde{\varepsilon}(\omega) = \varepsilon_c + (\omega_f/\omega)^2[f(\omega/2\Delta) - 1 - (\omega/2\Delta)^2 f^2(\omega/2\Delta)\lambda D_\varphi(\omega)]. \tag{19}$$

ω_f is a measure for the oscillator strength so that

$$\int_o^\infty \sigma(\omega)d\omega = (\pi/2)\,\varepsilon_o\omega_f^2. \tag{20}$$

2Δ is the Peierls gap and λ is the total electron-phonon coupling constant given by

$$\lambda = \sum_n \lambda_n = \sum_n g_n^2 N(\varepsilon_F)/\hbar\omega_n, \tag{21}$$

where n is the mode number.

Furthermore, the function, f(x), is defined by

$$f(x) = [\pi i + \ln(1-S)/(1+S)]/2Sx^2,\ S=(1-x^{-2})^{1/2} \tag{22}$$

A small electronic damping may be introduced by the substitution $x^2 \rightarrow x(x+i\delta)$ in these expressions. Finally, the phase phonon propagator

$$D_\varphi(\omega) = [D_o^{-1}(\omega) + 1 + \lambda(\omega/2\Delta)^2 f(\omega/2\Delta) + b],^{-1} \tag{23}$$

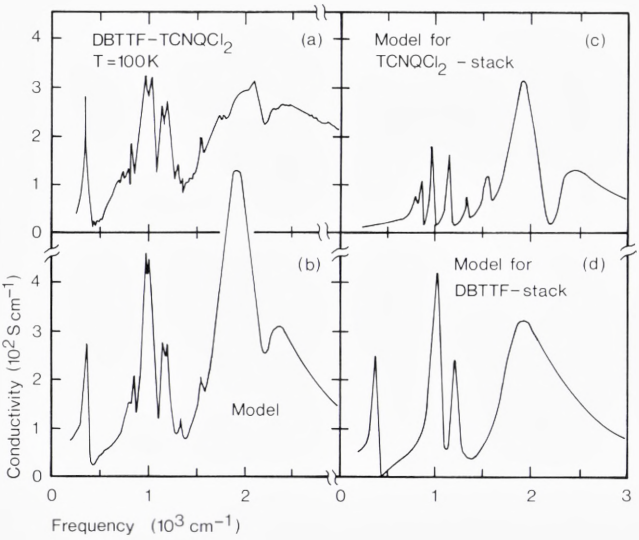

Fig. 13. $4k_F$-CDW model for $\sigma(\omega)$ of DBTTF-$TCNQCl_2$ at 100K. (a) data, (b) total $\sigma(\omega)$ in model, (c) contribution from acceptor stack, and (d) contribution from donor stack.

where

$$D_o(\omega) = -\sum_n (\lambda_n/\lambda)\omega_n^2/(\omega_n^2-\omega^2-i\omega\gamma_n). \tag{24}$$

γ_n is the natural damping rate of mode n. b is a positive constant, which models the pinning of the CDW; if b = 0, the CDW contributes to the dc conductivity.

The physical contents of this model were described previously. The main problem in its application to DBTTF-$TCNQCl_2$ is the double-stack structure. There are two contributing stacks and we must assume that $\tilde{\varepsilon}(\omega)$ is simply a sum of two individual terms. Clues to the decomposition may be obtained by studying single-stack materials like $DBTTF(BF_4)_{0.42}$. It is rather easy to show that DBTTF dominates the full spectrum and we have obtained a model fit to the data of the quality shown in Fig. 13(b). The individual contributions are pictured in Fig. 13 (c+d). The model parameters are given in Table VII, which also contains independent estimates of the emv coupling constants.

The overall quality of the fit is reasonable, especially with respect to distribution of oscillator strength between the vibrational modes and the single particle contribution. We note that it is possible to introduce only a modest electronic damping in the present model hence the gap structure in the fit is sharper than in the data.

From Table VII it follows that the coupling constants (g_n) obtained are of the correct magnitude. This is a crucial point, since in Eq. (21) we have used the $U\to\infty$ density of states, which for a quarter-filled band is

Table VII. $4k_F$-CDW parameters for DBTTF-$TCNQCl_2$, T = 100K.

	DBTTF			$TCNQCl_2$		
$\omega_f(cm^{-1})$	4500			3600		
4t(eV)	0.43			0.27		
$2\Delta(cm^{-1})$	1700			1900		
δ	0.2			0.2		
λ	0.46			0.60		
b	0.08			0.08		
$\Delta\varepsilon_c$	1.0			1.0		
n	ω_n cm^{-1}	λ_n	g_n[a] cm^{-1}	ω_n cm^{-1}	λ_n	g_n[b] cm^{-1}
1	1430	.16	1100 (940)	2253	.04	550(350)
2	1130	.017	320(170)	1573	.01	230(540)
3	473	.11	530(630)	1345	.01	210(500)
4	(40	.17	190)	1200	.04	400(300)
5				1020	.03	340(85)
6				870	.009	160
7				820	.012	180
8				(40	.45	250)

[a] values in parentheses are estimates for TTF for corresponding modes (Lipari et al., 1977).

[b] values in parentheses are estimates for TCNQ for corresponding modes (Rice et al., 1980).

only 35% of the U=0 value. Thus the strength of the vibrational modes constitutes a direct verification of the applicability of the large U model.

A few other points may be emphasized: (1) Assuming mean field behaviour the observed gap position corresponds to a scale temperature $T_{MF} \simeq 600K$. This is consistent with the well-established gap and CDW-structure at 300K and below. (2) In the fitting procedure the estimated gap-values were used to derive the total electron-phonon coupling constant, λ, from the gap equation (Eq.(15)) for each stack. Part of λ is assumed associated with low frequency (external) modes outside the experimental range (given in the last lines of Table VII). However, it is striking that more than 60% of λ for the DBTTF-stack is due to the internal modes. Hence, the CDW is predominantly stabilized by the emv

coupling. On the acceptor chain this is less pronounced. (3) The average bandwidth, $4\bar{t}$, is 0.35 eV from Table VII. This may be compared to $4\bar{t}$ = 0.41 eV from the Drude analysis (Table III). It appears that the oscillator strength is further reduced below what is expected from the large U model. Introduction of a finite nearest neighbour interaction, V, in the theory might account for that.

In conclusion the IR properties of DBTTF-$TCNQCl_2$ are surprisingly well described by the model for the large U, $4k_F$–Peierls system. The infrared properties of several singlestack conductors like $TMTTF_2PF_6$, and MEM-$TCNQ_2$ at 350K, may also be analysed satisfactory in terms of the same model (C. S. Jacobsen, to be published). Thus it appears that for a large group of organic conductors the electronic properties are reminiscent of those of a system, where double occupancy of sites is effectively excluded.

Sum rules and correlation effects

To investigate whether the infrared oscillator strength can give information on the strength of Coulomb correlations in general we give in Table VIII a comparison of the observed oscillator strength with the predicted in the $U=0$ and $U\rightarrow\infty$ limits for a number of compounds. In particular, the last column gives the ratio, β, between observed reduction of oscillator strength and the reduction associated with the $U\rightarrow\infty$ model. Thus $\beta=0$ corresponds to $U=V=0$ and $\beta=1$ to $U\rightarrow\infty$, $V=0$. It is notable that β is in no case smaller than 0.5. HMTSF-TCNQ and -TNAP, and $TMTSF_2ClO_4$, which are all excellent metals have β's close to 0.5. The semiconducting materials have $\beta\simeq 0.9$-1.3. TTF-TCNQ which will be discussed in more detail below has β = 0.85 decreasing to 0.56 at 60K, the temperature of maximum conductivity. This may indicate a connection between the absolute value of σ and the screening efficiency. A similar trend is observed in $ET_2I_3(\perp)$. However, here $\beta > 1$ in spite of the metallic ground state. The large β is attributed to the narrow (Table VI) and quarter-filled band. It appears that the metallic/superconducting ground state must be related to the 2D-nature of this material which precludes, for example, the $4k_F$-CDW instability.

The only material, which appears not to match the pattern is TMTSF-DMTCNQ, which has metallic character, but β = 1.1. We understand such a large β as arising from a Coulomb correlation dominated acceptor stack and a metallic donor stack as previously implied by analysis of the transport properties (Jacobsen et al., 1978).

Thus it largely appears that the β-values of Table VIII are consistent

Table VIII. Infrared oscillator strength and correlation effects. The first column gives the values expected if U=V=0 (based on Tables III and VI). The second column corresponds to U→∞, V=0 (Eq. 14), while the third gives the measured oscillator strength. β is a relative measure for the strength of the correlation effects (see text).

Material (temp.)	ω_p^2 ($10^7 cm^{-2}$)	$\omega_p^2 \cos\varrho\pi/2$ ($10^7 cm^{-2}$)	ω_f^2 ($10^7 cm^{-2}$)	β
TTF-TCNQ (300K)	13.0	8.4	9.1	0.85
TTF-TCNQ (60K)	15.9	9.5	12.3	0.56
TMTSF-DMTCNQ (300K)	12.5	8.8	8.5	1.08
HMTSF-TCNQ (300K)	20.2	8.0	13.0	0.59
DBTTF-$TCNQCl_2$(300K)	5.6	3.6	3.1	1.25
HMTSF-TNAP (300K)	12.8	7.8	10.3	0.50
$TMTTF_2PF_6$ (300K)	7.9	5.6	5.8	0.91
$TMTSF_2ClO_4$ (300K)	9.8	6.9	8.3	0.52
$ET_2I_3(\perp)$ (300K)	8.3	5.9	5.2	1.29
$ET_2I_3(\perp)$ (40K)	9.2	6.5	6.2	1.11

with independent information on the importance of correlation effects. The relatively big reduction of oscillator strength found indicates a considerable localization trend in the wavefunctions in full agreement with the enhancement in magnetic susceptibility generally observed (Torrance et al., 1977). The β-values, through Eq. (13), may prove useful in testing specific models for the wavefunctions in the intermediate correlation regime.

TTF-TCNQ: $2k_F$- and $4k_F$-instabilities

As the first good organic metal prepared, TTF-TCNQ remains one of the best characterized solids at all. Even so, many details remain controversial, one of them being the roles played by the two stacks. The physical and structural properties may briefly be summarized as follows:

The conductivity increases as T^{-2} or faster down to well below 100K (Cohen et al., 1974). At 60K σ(T) is sharply peaked, and from 53K and down a cascade of phase transitions destroys the metallic character. Extensive structural studies (see, for example, Comes and Shirane, 1979) have shown considerable 1D diffuse scattering at $4k_F$ from 300K and down to the phase transitions. Below 150K appreciable $2k_F$-scattering

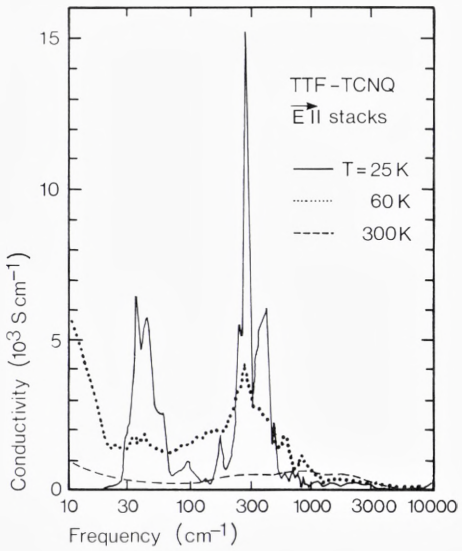

Fig. 14. Frequency dependent conductivity of TTF-TCNQ at 25K, 60K and 300K. Notice the logarithmic frequency scale. (Tanner and Jacobsen, 1982).

develops. The character is 1D to 53K, where it becomes 3D. Several physical properties indicate that the 53K transition takes place on the TCNQ-stacks and that the TTF-stacks follow at a lower temperature (Schultz and Craven, 1979). It also appears that the TCNQ-stacks carry most of the conductivity in this material. The magnetic susceptibility is enhanced by a factor 2-3 over the Pauli value at room temperature and decomposition into individual stack contributions tends to show that the TTF-stacks have most of the susceptibility. While these results agree with the bandwidth estimates of Table IV they disagree with a recent NMR study (Takahashi et al., 1984).

Here we will discuss the infrared properties in general and in particular try to assign the $2k_F$- and $4k_F$-instabilities to individual stacks. The overall infrared properties have recently been studied by Jacobsen (1979), Tanner et al. (1981), and Tanner and Jacobsen (1982). The temperature dependence of $\sigma(\omega)$ is shown in Fig. 14 in the entire infrared range. Eldridge and Bates (1983) have subsequently studied the low temperature, far infrared spectrum by a different technique. While their results are in general agreement with those shown here, details in especially the sharpness of the features differ.

At 25K, $\sigma(\omega)$ displays a double peak structure with a low frequency band near 40 cm^{-1} and a very intense band near 300 cm^{-1}. The low frequency band contains about 5% of the total oscillator strength. In view of the observed $2k_F$-superstructure and an energy gap estimated

from $\sigma_{dc}(T)$ of order 300 cm^{-1}, the intense band may be ascribed to single particle transitions across the gap in a $2k_F$-Peierls semiconducting state, while the 30 cm^{-1} band is assigned to the Fröhlich (i.e. CDW) pinned mode.

The CDW parameters estimated on basis of such an interpretation agrees with theoretical expectations (Tanner et al. 1981). However, a detailed fit of the spectrum in terms of the multiphonon theory previously employed is not yet possible.

The 60K spectrum shows a broadening of the 300 cm^{-1} structure and apparently the oscillator strength of the low frequency band has moved to zero frequency. Since $\sigma_{dc}(60K) \simeq 10^4 Scm^{-1}$, there is a sharp drop in $\sigma(\omega)$ in the millimetre and submillimetre range. Physically, this is consistent with a depinning of the CDWs at the phase transition. They appear to contribute to σ_{dc} and in the IR a pseudo-gap induced absorption, broadened by fluctuations, may be followed to temperatures above 100K. Going to 300K the features are much broadened and the maximum in $\sigma(\omega)$ has moved to about 800 cm^{-1}. The latter change can not be understood in terms of the $2k_F$-instability.

Instead we may focus on the role of the $4k_F$-instability which gives rise to the only detectable superstructure at 300K. It may be associated with only one or with both types of stack. As usual we expect the infrared properties of the $4k_F$-CDW to consist of a maximum in $\sigma(\omega)$ corresponding to a pseudogap plus a number of sharper features near the A_g-vibrational modes. TCNQ has such a mode near 2200 cm^{-1} (C ≡ N stretch), which couples strongly to the electrons. Fig. 15(a) shows a high resolution study of the reflectance near this mode. At 300K and 200K the feature has the strength and shape of an ordinary IR active mode superimposed on the metallic response of the conduction electrons. From 100K and down to 30K the oscillator strength increases and the shape is inverted (the original structure is presumably hidden behind the new band). The low temperature spectrum is exactly what is expected from a Peierls distorted semiconductor. The point is that the temperature dependence follows that of the $2k_F$-scattering. Thus the $4k_F$-instability must (at least largely) take place on the TTF-stacks. This conclusion agrees with recent diffuse X-ray studies on irradiated TTF-TCNQ (Forró et al., 1984).

It is also corroborated by a careful inspection of the far IR reflectance, shown in Fig. 15(b). Being raw data, these curves should be reliable with respect to position and relative strength of fine structure. Also shown is a model calculation for a $2k_F$-CDW system with $2\Delta = 300$ cm^{-1}, using the

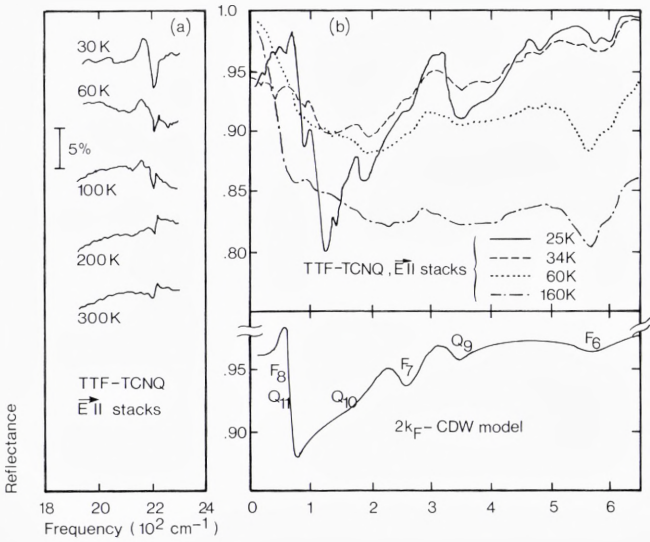

Fig. 15. Chain-axis reflectance of TTF-TCNQ. (a) Temperature dependence in the vicinity of the C≡N stretch frequency. (b) Temperature dependence in the far infrared (Tanner et al., 1981). At bottom is shown a $2k_F$-CDW model with identified A_g-mode features. Q refers to TCNQ, F to TTF.

known emv coupling constants of TTF and TCNQ (references from Table VII). The model mainly serves to identify the individual A_g-modes in the far infrared. It is again evident that TCNQ-modes (Q_{10}, Q_9) show a temperature dependence as that of the 2200 cm^{-1} mode, while the TTF-modes (F_6, F_7) are different. F_6 corresponds to a strong, near temperature independent dip in the reflectance from 160K to 60K. Below 60K it moves slightly up in frequency and becomes weaker with a different shape. This behaviour may tentatively be assigned to a cross-over from a $4k_F$- to a $2k_F$-CDW state on the TTF-chains.

The infrared properties are clearly consistent with the idea that the $2k_F$ (ordinary) Peierls instability develops on the TCNQ-chains and perhaps at low temperature induces $2k_F$-order on the TTF-chains as well. The $4k_F$-instability in contrast develops on the TTF-chains. This also agrees with the bandwidth estimates of Table IV. The rather narrow TTF-band is susceptible to a correlation induced $4k_F$-instability. The theory applied to the case of DBTTF-$TCNQCl_2$ is probably inappropriate, but qualitatively we may understand the 300K spectrum of TTF-TCNQ (see Fig. 11) as arising from a near Drude-like contribution from the TCNQ-stack and a contribution from the TTF-stack, which has a maximum near 800 cm^{-1} and emv interference effects in the 1400-1500 cm^{-1} range, where the important carbon skeleton modes are situated (compare Table VII). Interestingly, the rise in $\sigma(\omega)$ at low frequencies may arise from sliding $4k_F$-CDWs, which here (in contrast to the case of DBTTF-

$TCNQCl_2$) experience no Coulomb scattering from oppositely charged density waves.

Conclusions

In the above study we have completed the following line of argumentation: It was shown empirically that the plasma edge Drude analysis of organic conductors yields reliable estimates for bandwidths. This in particular means that the plasmon frequency is largely insensitive to the often strong deviations from Drude behaviour encountered at low frequencies.

By comparing the bandwidth values with the integrated intraband oscillator strength, information on the importance of short range Coulomb correlations was extracted. It appears that all organic conductors have prominent »Coulomb holes«, but clear differences are found between good metals and moderate conductors. For the latter, models where double occupancy of sites is excluded have proven useful in explaining the semiconducting nature. In other materials, where Coulomb correlation effects appear equally strong, interchain interactions preserve the metallic character to low temperature, where even superconductivity may be found (as exemplified by ET_2I_3).

Finally, those molecular vibration modes, which couple to the electrons, were used as »fingerprints« to understand the nature of TTF-TCNQ, where apparently one chain-type shows much stronger correlation effects than the other.

ACKNOWLEDGMENTS. *This work could not have been done without the continuing collaboration with K. Bechgaard, who supplied most of the samples studied.*

Other samples were prepared by J. R. Andersen, I. Johannsen, M. Albjerg, L. Groth-Andersen, and H. Wang.

Some of the infrared measurements (far IR studies on TTF-TCNQ and all measurements on $TMTSF_2PF_6$) have been done jointly with D. B. Tanner, who also contributed to the interpretation. The author acknowledges helpful discussions with many collaborators and colleagues, among them especially K. Mortensen, H. J. Pedersen, K. Carneiro, R. Bozio, P. M. Grant, M. J. Rice, J. B. Torrance, J. M. Williams, and V. M. Yartsev. He also thanks G. Rindorf, H. Soling, and N. Thorup for expertise help in all matters regarding crystallography. M. H. Jørgensen and J. Schjær-Jacobsen were instrumental in the automation of the IR spectrometer, which saved much time subsequently.

This work has been partially financed by the Danish Natural Science Research Council and the NATO Research Grants Programme.

References

Allen, P. B. (1971) Phys.Rev. B *3,* 305.

Andersen, J. R., Bechgaard, K. Jacobsen, C. S., Rindorf, G., Soling, H., and Thorup, N. (1978) Acta Cryst. B *34,* 1901.

Baeriswyl, D., Harbeke, G., Kiess, H., and Meyer, W. (1982) In *Electronic Properties of Polymers,* ed. by Mort, J. and Pfister, G. (Wiley, New York), p. 267.

Bardeen, J., Cooper, L. N., and Schrieffer, J. R. (1957). Phys.Rev. *106,* 162; *108,* 1175.

Bechgaard, K., Kistenmacher, T. J., Bloch, A. N., and Cowan, D. O. (1977). Acta Cryst. B *33,* 417.

Bechgaard, K., Jacobsen, C. S., and Andersen, N. H. (1978). Solid State Commun. *25,* 875.

Bechgaard, K., Jacobsen, C. S., Mortensen, K., Pedersen H. J., and Thorup, N. (1980). Solid State Commun. *33,* 1119.

Bechgaard, K., Carneiro, K., Olsen, M., Rasmussen, F. B., and Jacobsen, C. S. (1981a). Phys.Rev. Lett. *46,* 852.

Bechgaard, K., Carneiro, K., Rasmussen, F. B., Olsen, M., Rindorf, G., Jacobsen, C. S., Pedersen, H. J., and Scott, J. C. (1981b). J.Am.Chem.Soc. *103,* 2440.

Bernasconi, J., Rice, M. J., Schneider, W. R., and Strässler, S. (1975). Phys.Rev. B *12,* 1090.

Bloch, A. N., Cowan, D. O., Bechgaard, K., Pyle, R. E., Banks, R. H., Poehler, T. O. (1975). Phys.Rev.Lett. *34,* 1561.

Bosch, A., and van Bodegom, B. (1977). Acta Cryst. B *33,* 3013.

Bozio, R., and Pecile, C. (1980). In *The Physics and Chemistry of Low Dimensional Solids,* L. Alcácer, ed. (Reidel, Dordrecht), p. 165.

Bright, A. A., Garito, A. F., and Heeger, A. J. (1974). Phys.Rev. B *10,* 1328.

Bryden, W. A., Kistenmacher, T. J., Poehler, T. O., Chappell, J. S., Emge, T. J., Lee, M. M., Lerstrup, K. A., Wiygul, F. M., Cowan, D. O., Stokes, J. P., and Bloch, A. N. (1984). Phys.Rev. B, to be published.

Chaikin, P. M., Greene, R. L., Etemad, S., and Engler, E. (1976). Phys.Rev. B *13,* 1627.

Chesnut, D. B. (1966). J.Chem.Phys. *45,* 4677.

Cohen, M. J., Coleman, L. B., Garito, A. F., and Heeger, A. J. (1974). Phys.Rev. B *10,* 1298.

Comès, R., and Shirane, G. (1979). In *Highly Conducting One-Dimensional Solids,* J. T. Devreese, R. P. Evrard, and V. E. van Doren, eds. (Plenum Press, N.Y.), p. 17.

Conwell, E. M. (1980). Phys.Rev. B *22,* 1761.

Delhaes, P., Coulon, C., Amiell, J., Flandrois, S., Toreilles, E., Fabre, J. M., and Giral, L. (1979). Mol.Cryst. Liq.Cryst. *50,* 43.

Duke, C. B., Lipari, N. O., and Pietronero, L. (1975). Chem.Phys.Lett. *30,*415.

Eldridge, J. E., and Bates, F. E. (1983). Phys.Rev. B *28,* 6972.

Etemad, S., Penney, T., Engler, E. M., Scott. B. A., and Seiden, P. E. (1975). Phys.Rev. Lett. *34,* 741.

Ferraris, J., Cowan, D. O., Walatka, V., and Perlstein, J. H. (1973). J.Am.Chem.Soc. *95,* 948.

Forró, L., Bouffard, S., and Pouget, J. P. (1984). J.Phys. (Paris) Lettr. *45,* L543.

Fröhlich, H., (1954). Proc. Royal Soc. (London) *A223,* 296.

Grant, P. M. (1983). J.Phys. (Paris)-Colloq. *44,* C3-847.

Greene, R. L., Mayerle, J. J., Schumaker, R., Castro, G., Chaikin, P. M., Etemad, S., and LaPlaca, S. J. (1976). Solid State Commun. *20,* 943.
Gutmann, F., and Lyons, L. E. (1967). *Organic Semiconductors* (Wiley, New York).
Herman, F. (1977). Physica Scripta *16,* 303.
Holstein, T. (1954). Phys.Rev. *96,* 535.
Holstein, T. (1964). Ann.Phys. (N.Y.) *29,* 410.
Horovitz, B., Gutfreund, H., and Weger, M. (1975). Phys.Rev. B *12,* 3174.
Hubbard, J. (1978). Phys. Rev. B *17,* 494.
Huizinga, S., Kommandeur, J., Sawatzky, G. A. Kopinga, K., de Jonge, W. J. M. (1979). Lecture Notes in Physics *96,* 45.
Jacobsen, C. S. (1979). Lecture Notes in Physics *95,* 223.
Jacobsen, C. S., Mortensen, K., Andersen, J. R., and Bechgaard, K. (1978). Phys.Rev. B *18,* 905.
Jacobsen, C. S., Pedersen, H. J., Mortensen, K., and Bechgaard, K. (1980). J.Phys.C.: Solid St.Phys. *13,* 3411.
Jacobsen, C. S., Tanner, D. B. and Bechgaard, K. (1981). Phys.Rev.Lett. *46,* 1142.
Jacobsen, C. S., Tanner, D. B., and Bechgaard, K. (1983). Phys.Rev. B *28,* 7019.
Jacobsen, C. S., Johannsen I., and Bechgaard, K. (1984). Phys.Rev.Lett. *53,* 194.
Jacobsen, C. S., Williams, J. M., and Wang, H. H. (1985). Solid State Commun. *54,* 937.
Jerome, D., and Schulz, H. J. (1982). Advances in Physics *31,* 299.
Jerome, D., Mazaud, A., Ribault, M., and Bechgaard, K. (1980). J.Phys. (Paris), Lett. *41,* L95.
Kagoshima, S., Ishiguro, T., and Anzai, H. (1976). J.Phys.Soc.Jpn. *41,* 2061.
Kaminskii, V. F., Prokhorova, T. G., Shibaeva, R. P., and Yagubskii, E. B. (1984). Pis'ma Zh.Eksp.Teor.Fiz. *39,* 15 (JETP Lett. *39,* 17).
Kistenmacher, T. J. (1978). Ann.N.Y.Acad.Sci. *313,* 333.
Kistenmacher, T. J., Phillips, T. E., and Cowan, D. O. (1974). Acta Cryst. B *30,* 763.
Koch, B., Geserich, H. P., Ruppel, W., Schweitzer, D., Dietz, K. H., and Keller, H. J. (1985). Mol.Cryst.Liq.Cryst., *119,* 343.
Lerstrup, K., Lee, M., Wiygul, F. M., Kistenmacher, T. J., and Cowan, D. O. (1983). J.Chem.Soc.Chem.Commun. 294.
Liautard, B., Peytavin, S. Brun, G., and Maurin, M. (1982). J.Phys. (Paris) *43,* 1454.
Lieb, E. H., and Wu, F. Y. (1968). Phys.Rev.Lett. *20,* 1445.
Lipari, N. O., Rice, M. J., Duke, C. B., Bozio, R., Girlando, A., and Pecile, C. (1977). Int.J. Quantum Chem.: Quantum Chem.Symp. *11,* 583.
Lyo, S. K. (1978). Phys.Rev. B *18,* 1854.
Lyo, S. K., and Gallinar, J.-P. (1977). J.Phys.C: Solid St.Phys. *10,* 1696.
Maldague, P. F. (1977). Phys.Rev. B *16,* 2437.
Mazumdar, S., and Bloch, A. N. (1983). Phys.Rev.Lett. *50,* 207.
Megtert, S., Pouget, J. P., Comès, R. Garito, A. F., Bechgaard, K., Fabre, J. M., and Giral, L. (1978). J.Phys. (Paris) *39,* L-118.
Mortensen, K. (1982). Solid State Commun. *44,* 643.
Mortensen, K., Jacobsen, C. S., Lindegaard-Andersen, A., and Bechgaard, K. (1983). J.Phys. (Paris) Colloq. *44,* C3-1349.
Mortensen, K., Jacobsen, C. S., Bechgaard, K., Carneiro, K., and Williams, J. M. (1985). Mol.Cryst.Liq.Cryst., *119,* 401.

Mott, N. F. (1949). Proc.Phys.Soc. (London) *A62,* 416.
Overhauser, A. W. (1960). Phys.Rev.Lett. *9,*462.
Peierls, R. E. (1955). *Quantum Theory of Solids* (Oxford Univ. Press), p. 108.
Phillips, T. E., Kistenmacher, T. J., Bloch, A. N., and Cowan, D. O. (1976). J.Chem. Soc.Chem.Commun. 334.
Pines, D. (1964). *Elementary Excitations in Solids.* (Benjamin, New York).
Pouget, J. P. (1981). Chemica Scripta *17,* 85.
Pouget, J. P. (1984). Unpublished work.
Rice, M. J. (1978). Solid State Commun. *25,* 1083.
Rice, M. J. (1979). Solid State Commun. *31,* 93.
Rice, M. J., and Strässler, S. (1973). Solid State Commun. *13,* 125.
Rice, M. J., Duke, C. B. and Lipari, N. O. (1975). Solid State Commun. *17,* 1089.
Rice, M. J., Pietronero, L., and Brüesch, P. (1977). Solid State Commun. *21,* 757.
Rice, M. J., Yartsev, V. M., and Jacobsen, C. S. (1980). Phys.Rev. B *21,* 3437.
Ritsko, J. J., Sandman, D. J., Epstein, A. J., Gibbons, P. C., Schnatterly, S. E., and Fields, J. (1975). Phys.Rev.Lett. *34,* 1330.
Schultz, A. J., Stucky, G. D., Blessing, R. H., and Coppens, P. (1976). J.Am.Chem.Soc. *98,* 3194.
Schultz, T. D., and Craven, R. A. (1979). In *Highly Conducting One-Dimensional Solids,* J. T. Devreese, R. P. Evrard, and V. E. van Doren, eds. (Plenum Press, N.Y.), p. 147.
Slater, J. C. (1951). Phys.Rev. *82,* 538.
Sokoloff, J. B. (1970). Phys.Rev. B *2,* 779.
Soling, H., Rindorf, G., and Thorup, N. (1981a). Acta Cryst. B *37,* 1716.
Soling, H., Rindorf, G., and Thorup, N. (1981b). Unpublished work.
Tajima, H., Yakushi, K., Kuroda, H., Saito, G., and Inokuchi, H. (1984). Solid State Commun. *49,* 769.
Takahashi, T., Jerome, D., Masin, F., Fabre, J. M., and Giral, L. (1984). J.Phys. C: Solid State Phys. *17,* 3777.
Tanaka, J., Tanaka, M., Tanaka C., Ohno, T., Takabe, T., and Anzai, H. (1978). Ann. N.Y. Acad.Sci. *313,* 256.
Tanner, D. B., and Jacobsen, C. S. (1982). Mol.Cryst.Liq.Cryst. *85,* 137.
Tanner, D. B., Jacobsen, C. S., Garito, A. F., and Heeger, A. J. (1976). Phys.Rev. B *13,* 3381.
Tanner, D. B., Cummings, K. D., and Jacobsen, C. S. (1981). Phys.Rev. Lett. *47,* 597.
Thorup, N., Rindorf, G., Soling, H., and Bechgaard, K. (1981). Acta Cryst. B *37,* 1236.
Torrance, J. B. (1979). Acc.Chem.Res. *12,* 79.
Torrance, J. B., Tomkiewicz, Y., and Silverman, B. D. (1977). Phys.Rev. B *15,* 4738.
Weyl, C., Engler, E. M., Bechgaard, K., Jehanno, G., and Etemad, S. (1976). Solid State Commun. *19,* 925.
Williams, P. F., and Bloch, A. N. (1974). Phys.Rev. B *10,* 1097.
Wooten, F. (1972). *Optical Properties of Solids* (Academic Press, New York).
Yagubskii, E. B., Shchegolev, I. F., Laukhin, V. N., Kononovich, P. A., Karatsovnik, M. V., Zvarykina, A. V., and Buravov, L. I. (1984). Pis'ma Zh.Eksp.Teor.Fiz. *39,* 12 (JETP Lett. *39,* 12).
Yamaji, K. (1985). Mol.Cryst.Liq.Cryst., *119,* 105.